International Journal of Engineering Trends and Technology
ISSN: 2231–5381 / https://doi.org/10.14445/22315381/IJETT-V72I3P120

Volume 72 Issue 3, 218-229, March 2024

Original Article

Synthesis of Corrosion Inhibitor Based on Polymethyl Methacrylate and Investigation of Inhibition Efficiency on Carbon Steel in a 1 M HCl Medium

Choriev I.K[1], Turaev Kh. Kh[2], Normurodov B.A[3], Muzaffarova N. Sh[4], Mukumova G.J[5], Kholboeva A. I[6]

[1]*Faculty of Applied Mathematics and Intellectual Technologies, Termez, Uzbekistan.*
[2,3,5,6]*Faculty of Chemistry, Termez State University, Termez, Uzbekistan.*
[4]*Department of Medical and Biological Chemistry, Termez Branch of Tashkent Medical Academy, Termez, Uzbekistan.*

[1]*Corresponding Author : abrornomozov055@gamil.com*

Received: 06 January 2024 Revised: 14 February 2024 Accepted: 23 February 2024 Published: 17 March 2024

Abstract *- The newly composite corrosion inhibitors have been synthesized from monoethanolamine, methyl methacrylate, and phosphoric acid, and their inhibition efficiency was studied. In this case, the mole ratio of the initial substances was maintained at 1:2:2, respectively, and the temperature remained between 35 ^{0}C and 40 ^{0}C, and 48 hrs. time duration was also been followed. The composition of this obtained composite corrosion inhibitor was studied by spectroscopic techniques and also quantum chemical calculation. In addition, the decomposition rate was determined using DTA and TGA processes. Moreover, the inhibition efficiency of this corrosion inhibitor (MMF-1) was studied using electrochemical measurements at different temperatures and concentrations. Polarization measurements have been carried out, and analysis of anodic and cathode slopes of polarization curves has shown that this inhibitor is a mixed-type inhibitor. Furthermore, the formation of protective films on carbon steel surfaces was confirmed by analyzing scanning electron microscopy and atomic force microscopy. Specially inhibition mechanism of this corrosion inhibitor was widely studied at temperatures of 298, 303, 313, and 323 K and unequivocally confirmed that it follows the Langmuir adsorption isotherm.*

Keywords *- Corrosion inhibitor, Monoethanolamine, Methyl methacrylate, Phosphoric acid.*

1. Introduction

Corrosion is a reversible process which converts pure metal to different chemical compounds[1]. Nowadays, corrosion is turning into a major issue in many industries, including building materials, infrastructure, tools, ships, trains, vehicles, machines, and appliances[2]. Carbon steel experiences extensive corrosion with acids during the cleansing process. The NACE 2016 reported that across the world, about 2.5 trillion U.S. dollars in economic fall due to corrosion and Every year, 10% of metal is lost due to corrosion, which severely affects the country's economy [3,4]. Corrosion is not only responsible for economic loss but is also related to safety issues because it decreases the shelf life of steel[5,6]. It has already been recognized as a major issue for the entire world, so researchers are trying to protect the corrosion process in various ways [7]. Mostly, inhibitors are typically used to protect the metal from corrosion. Environmentally friendly inhibitors have wide applications in corrosion fields and are generally added to metals at a low concentration[8,9]. This study is a small initiative to find a suitable corrosion inhibitor to protect materials from the corrosion process. According to this study, corrosion inhibitors were prepared based on poly(methyl methacrylate-maleic anhydride) P(MMA-MAH)s accompanied with different percentages of methyl methacrylate and maleic anhydride and the inhibitory potentiality of this inhibitor has checked on simple carbon steel in a 0.5 M HCl [10,11].

2. Material and Methods

2.1. Materials

To synthesize this composite corrosion inhibitor, monoethanolamine and methyl methacrylate monomers (purified by driving in an inert nitrogen atmosphere) and phosphoric acid, such as 1 M HCl for aggressive environments, were used. Steel composition: Fe 97.755-97.215%, C 0.17-0.24%, Si 0.17-0.37, Mn 0.35-0.65%, Ni 0.3%, S 0.04 %, P 0.035 %, Cr 0.25 %, Cu 0.3 %, As 0.08 %. 2×2.5 cm2 samples of steel with this composition were taken, and the surface was cleaned with sandpapers, washed several times in acetone and dried.[12]

2.2. Methods

Analytical results are obtained using different types of analytical instruments, which are mentioned with

specifications below:

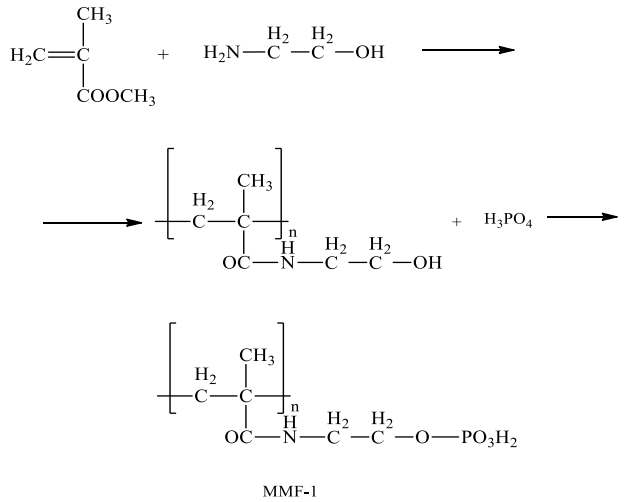

Fig. 1 The synthetic route used in the preparation of inhibitor MMF-1

Infrared Spectroscopic (IR) technique - IR Spectra, Specially synthesized Corrosion Inhibitors are checked by "IRTracer-100" (SHIMADZU CORP., Japan, 2017) Spectrometer. Scanning Electron Microscope (SEM, Smart SEM software SEM-EVO MA 10 (Carl Zeiss, Germany)) and thermal stability in differential-thermal and thermogravimetric methods of France analyzed on a LABSYS EVO STA devices are used. NMR spectra on JNM-ECZ600R spectrometer (JEOL, Japan), Atomic Force Microscopy (AFM) were used, and electrochemical studies were performed using devices such as the CS-350 Corrosion test.

3. Experimental Part

3.1. Synthesis of MMF-1 Composite Corrosion Inhibitor based on Methyl Methacrylate, Monoethanolamine and Phosphoric Acid

MMF-1 composite corrosion inhibitor was prepared from 1 mol of methyl methacrylate (102 g) and 2 mol (122 g) of monoethanolamine, were placed in a 250 cm^3 round-bottomed flask and refluxed in a furnace equipped with a magnetic stirrer at a temperature between 35 ^{0}C and 40 ^{0}C within 48 hours duration. The product was pumped out using a hermetically sealed device at a pressure of 0.8 Pa. Later, it was mixed with 2 mol (196 g) of phosphoric acid for 1.5 hours until a homogeneous mass was formed.

3.2. IR-Analysis

IR spectra of the obtained inhibitor were run, and several peaks at particular regions for individual functional groups were found. According to the results, it has revealed that the valence vibrations of the -C-H bond in the methyl (-CH_3) group were observed at 2939,52 $cm^{-1,}$ and the –C-H bond in the methylene (-CH_2-) group got at 2866.22 cm^{-1}. In addition, that - N-H bonds were observed in the area of 3356.14 cm^{-1}. Moreover, the –OH and -O-CH_3 group peaks were found at 3290.56 and 1653.0 cm^{-1} respectively.

3.3. Analysis of Results of ^{1}HNMR and ^{13}CNMR Analysis

The ^{1}HNMR and ^{13}CNMR graphs are included in Figure 2 and Figure 3, respectively. The ^{1}HNMR and ^{13}CNMR analyses of the obtained inhibitor were carried out, and a discussion of the results is clearly included in the paper.

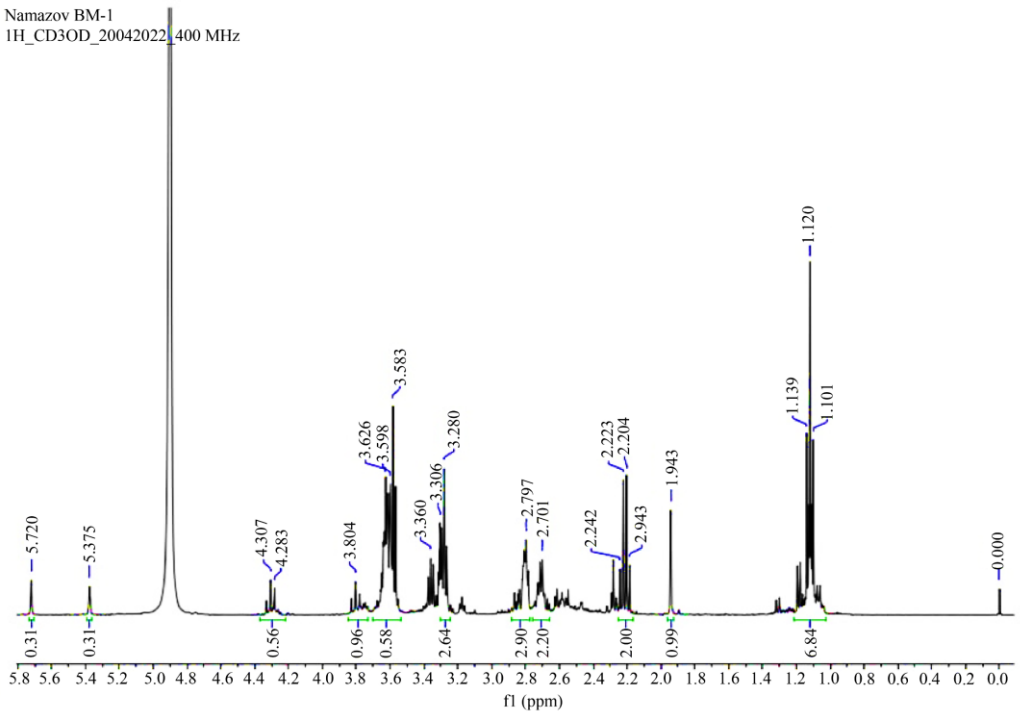

Fig. 2 ^{1}H NMR spectrum of the synthesized corrosion inhibitor compound

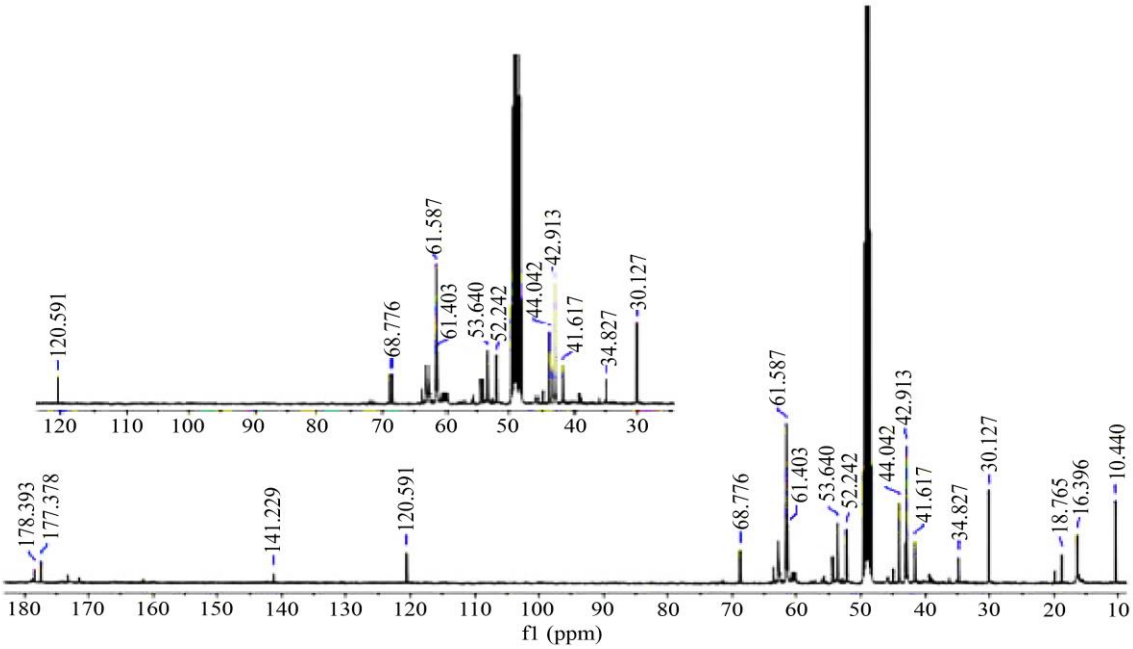

Fig. 3 ^{13}C NMR spectrum of the synthesized corrosion inhibitor

According to the ^{1}H NMR graph, it is evident that two CH_2 groups bonded with O and also N have exhibited peaks at 3.804 ppm and 3.6 ppm, respectively. In addition, other CH_2 and CH_3 group peaks are firmly observed below at 1.5 ppm. Moreover, another major NH peak of the compound did not appear in the scale, most probably because the NH protons could able to exchange with deuterium. The peak might be diminishing or disappear [Anthony Foris, On NH NMR Chemical Shifts part 1, For further confirmation of the compound, we have run ^{13}C NMR spectrum of our obtained inhibitor. In the ^{13}C NMR, quaternary carbon that was bonded to the NH group showed a peak at 177.37 ppm, and the carbon of the CH_2 group bonded to the NH group (C- 6) exhibited a peak at – 39.6 ppm. Furthermore, the carbon peak of the CH_2 group, which bonded with O and another CH_2 group, was also found at – 61.58 ppm, and another quaternary carbon bonded with the methylene group, and the CH_3 group showed a peak at -43. 7 ppm.

3.4. Quantum-Chemical Calculations

The resulting corrosion inhibitor geometries were created using the Avogadro software package and fully optimized by the Pople basis set -RHF/6-31G(d,p) and Gauss View 6.0.16 software. The Gauss View 6.0.16 calculations have been followed using the DFT (B3LYP) method and also the Mulliken method. Usually, density functional theory, DFT is applied to calculate quantum chemical parameters such as the highest occupied molecular orbital energy, the lowest unoccupied molecular orbital energy, electron affinity, global electrophilicity index, the fraction of electron transferred, global nucleophilicity index, and Mulliken charges. The Frontier Molecular Orbital (FMO) approximation has been calculated for the charges of all atoms and visualized using the Avogadro program. The comparison of the values of electronic charges was clearly obtained from the calculations referring to the methods and concluded that donor atoms with the highest values of negative charge in all calculated molecules could able to coordinate.

3.5. Study of Thermal Properties of MMF-1 Brand Composite Corrosion Inhibitor

The MMF-1 composite corrosion inhibitor was synthesized at a maximum 800 °C temperature in a dry mass, which is presented in Figure 1, and the results of the pigment analysis were studied according to the given thermogravimetric derivatogram (TGA) and differential thermogravimetric analysis. TGA and DTA thermogravimetric analyses (Figure 4) of MMF-1 brand composite corrosion inhibitor were conducted by SHIMADZU DTG-60 thermal analysis device in the 20-800 °C temperature range. All samples of the thermal analysis of the MMF-1 brand composite corrosion inhibitor have been followed in a dynamic mode at a speed of 10 degrees/min in an aluminum mortar. The TGA-DTA curves, as shown in Figure 4, indicate the occurrences of weight losses at particular temperature ranges. In fact, Thermal analytical techniques such as Thermogravimetric Analysis (TGA), Differential Thermal Analysis (DTA), and Differential Scanning Calorimetry (DSC) are useful tools to detect the physical changes in a material which include mass loss, thermal decomposition, and phase changes as a function of temperature and time. So, this thermal analysis provides thermal stability and phase stability of our obtained composite corrosion inhibitor.

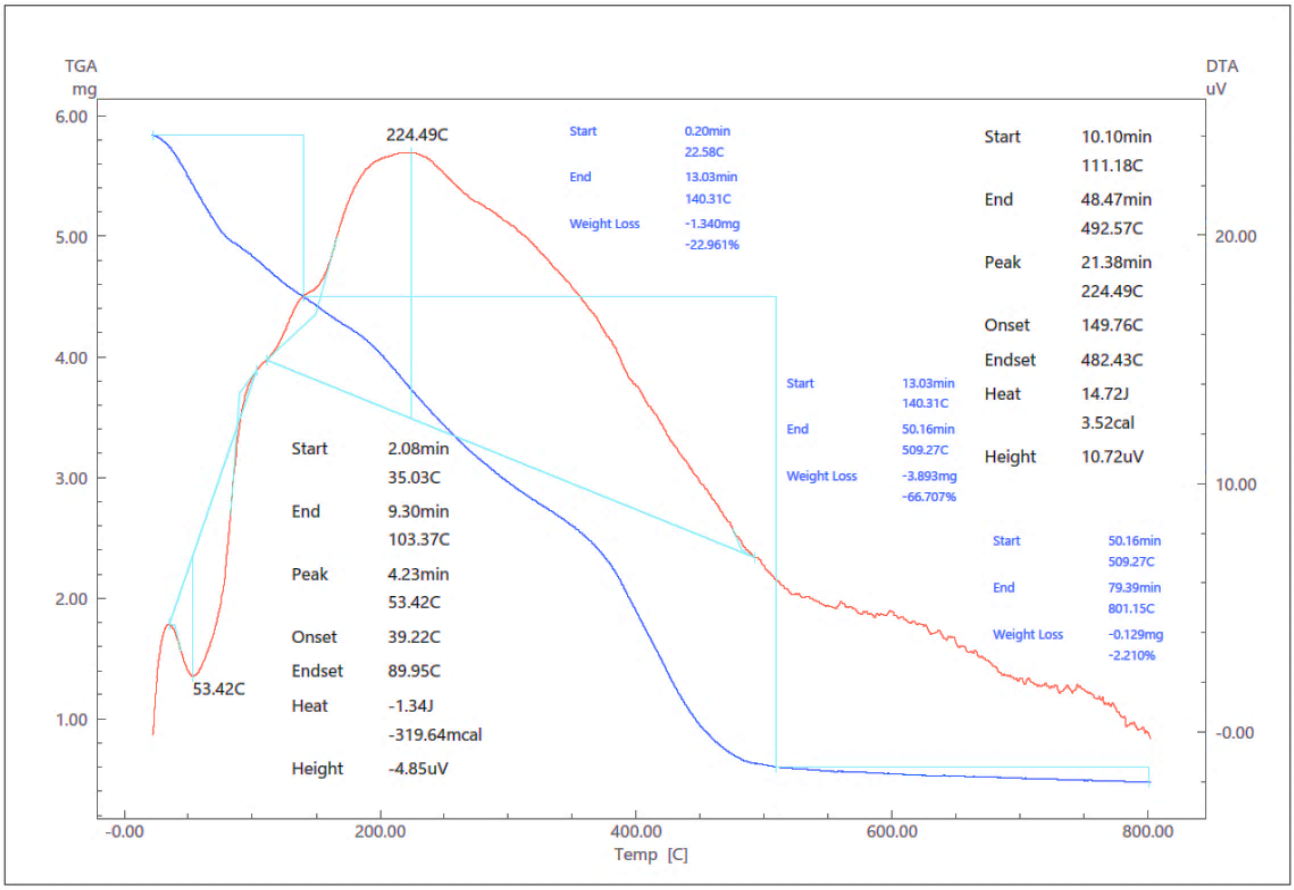

Fig. 4 Thermogravimetric analysis (TGA) and Differential thermogravimetric analysis (DTA) of MMF-1 composite corrosion inhibitor

The exothermic and endothermic effects were observed at 224.49 °C and 53.42 °C, respectively. The 5.836 mg amount of MMF-1 brand composite corrosion inhibitor was taken in an open-mouth crucible made of aluminum resistant to a temperature of 800 °C, and the temperature was gradually increased starting from 20 °C and intensive mass losses were found according to the TGA curve. Significant mass loss intervals 1, 2, and 3 were measured at 22.58 – 140.3 °C, 140.3 – 509.3 °C, and 509.3 – 800 °C, respectively. According to the analysis, it clearly showed that mass loss and percentages for moss loss intervals 1, 2 and 3 were found to be 1.34 mg (22.9%), 3.89 mg (66.7%) and 0.129 mg (2.2%), respectively. Differential thermogravimetric analysis of MMF-1 composite corrosion inhibitor is presented in Figure 4 and exhibited that the energy absorption has occurred in the range of 35.4 - 103.37 °C. The highest heat absorption occured at a temperature of 53.42 °C, and the energy release was found in the range of 111.18 - 492.57 °C. The highest heat output was found at a temperature of 224.49 °C.

The analysis of the results of the thermal decomposition of the substance at different temperatures is given in Table 1.

Table 1. Analysis of TGA and DTA curve results of MMF-1 brand composite corrosion inhibitor

No	Temperature,°C	Lost mass, mg (5,836 mg)	Loss of mass, mg, %	The amount of energy consumed (µV*s/mg)	Time spent (min)	dw (mg)	dw/dt (mg/min)
1	100	1,006	17,23	14.27	8,9	4.83	0,1
2	200	1,8	30,8	23.05	18,9	4.022	0,09
3	300	2,8	47,9	20.48	28,9	2.957	0,09
4	400	3,9	66,8	13.9	39,06	1.889	0,09
5	500	5,2	89,1	6.65	49,23	0.612	0,1
6	600	5,29	90,6	4.8	59,23	0.542	0,08
7	700	5,3	90.8	2,12	69,1	0,504	0,07
8	800	0,47	8,05	0,03	79,3	0,47	0,1

Table 2. Electrochemical impedance spectroscopy parameters of St20 in different concentrations of MMF-1 compounds and 1.0 M HCl solutions without inhibitor at 298 K

Inhibitor	Inhibitor Concentration mg/l	E_a, kJ/mol	ΔH* kJ/mol	ΔS* kJ/mol·K
Without an inhibitor	0,00	-54,38	-53,69	-12,37
MMF-1	50	-97,56	-94,52	-121,64
	100	-106,67	-101,79	-144,68
	200	-125,31	-122,36	-203,56
	500	-144,89	-137,65	-262,17

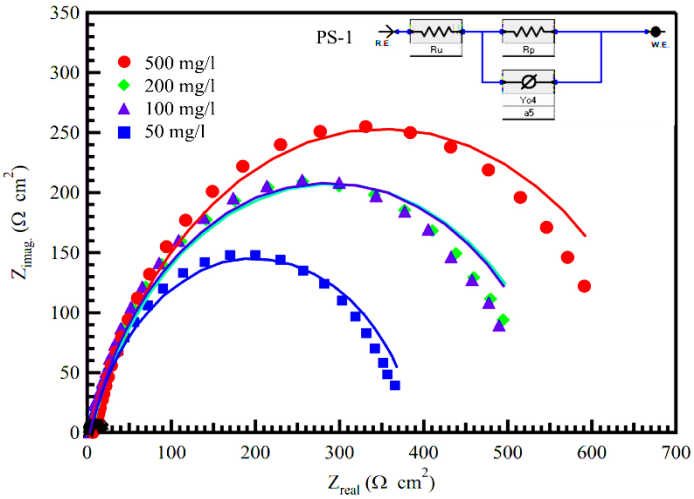

Fig. 5 Nyquist plots of St20 steel in solutions in 1.0 M HCl without and in the presence of different concentrations of the MMF-1 inhibitor at 298 K (The inset displays the equivalent circuit model utilized to fit the EIS data, and the solid line represents the fitting data.)

From the results of TGA and DTA, we know that this composite corrosion inhibitor can be used in environments above 150 ^{0}C.

4. Results and Discussion

4.1. Electrochemical Studies

Electrochemical Impedance Spectroscopy (EIS) measurements are a valuable method for characterizing various electrochemical systems and understanding the function of electrolytic processes such as batteries and the behavior of molecules during corrosion. Figure 5 shows the Nyquist plots of St20 at different concentrations for the corrosion study [13,14]. The curved rings showed that the corrosion of St20 steel and the formation of surface barriers were mainly controlled by the electron transfer process. The equivalent circuit model is shown in Figure 5 and was used to compare the experimental data on the impedance of St20 steel in the presence of inhibitors in 1 M HCl. According to the model, the solution resistance Rs, charge transfer resistance, R_{ct} and the double layer capacitance (C_{dl}) on the metal surface were determined.

Table 2 clearly explains that when additives were added to the 1M HCl solution, resistance to charge transfer, Rct, and values for ST20 increased, and as a result, the charge transfer pathways were hindered [13,15]. Inhibition efficiency, IE(EIS) and θ were calculated using the following formula (1 and 2):

$$E_{EIS} = \theta \times 100 = \left[\frac{R_{ct(inh)} - R_{ct(ninh)}}{R_{ct(inh)}}\right] \times 100 \qquad (1)$$

Here: R_{ct}(inh) and R_{ct}(ninh) were resistant to charge transfer in the presence and absence of inhibitor, respectively.

$$C_{\text{dl}} = (Y_0 R_{ct}^{1-n})^{\frac{1}{n}} \qquad (2)$$

Where n was the Constant Phase Element (CPE) indicator, and Y_0 was the CPE constant. n value between 0 and 1 was represented a deviation from ideal behavior. When the inhibitor was applied, the value of Cdl decreased, which indicated the decrease of the local dielectric constant and increased the thickness of the electrical double layer due to the formation of a protective layer on the metal surface [17,18].

Electrochemical Frequency Modulation (EFM) is an electrochemical method for calculating corrosion rates without prior knowledge of Tafel constants. Electrochemical Frequency Modulation (EFM) has attracted the attention of corrosion researchers as a promising technique with high sensitivity due to the measurement of corrosion parameters at harmonics and intermodulations of input frequencies, as well as high accuracy due to the inherent calculation of causality factors. The ability of this method is to estimate corrosion rates, Tafel parameters, and causal factors in a single data set. Table 3 shows the corrosion parameters for protection efficiency, corrosion current density, Tafel constant, and causal factors (CF-2) and (CF-3) for different concentrations in 1M HCl at 298 K[19-23].

Table 3. EFM parameters of CT20 in 1.0 M HCl in the absence and presence of different concentrations of compounds MMF-1 at 298 K

Inhibitor	C	I_{corr}	βa	βc	K	CF (2)	CF (3)	θ	% IE (EFM)
	mg/l	(uA)	(mV dec^{-1})	(mV dec^{-1})	mm·y				
Without an inhibitor	–	1071	72,53	94,36	459,87	2,12	3,24	0,92	92,31
MMF-1	50	82,64	52,41	61,25	39,62	1,63	1,95	0,93	93,42
	100	74,22	47,62	49,54	32,44	1,49	2,46	0,94	94,33
	200	60,56	29,54	33,17	26,53	1,15	2,97	0,95	95,15
	500	49,67	15,75	21,48	23,69	1,08	3,12	0,96	96,48

Table 4. Corrosion parameters obtained from potentiodynamic polarization measurements of St2 steel in 1.0 M HCl at different concentrations of MMF-1 inhibitor at 298 K

Inhibitor	C, mg/l	βa ($mV\ dec^{-1}$)	βc ($mV\ dec^{-1}$)	I_{corr}, (uA)	Ecorr vs. SCE	K (mpy)	Chi Squared	θ	IE
Without an inhibitor	–	315	187	4076	-342	1822	87,62	–	–
MMF-1	50	214	238	409	-406	175,6	72,36	0,91	91,13
	100	237	223	316	-418	138,4	68,45	0,92	92,37
	200	221	289	253	-422	116,3	79,64	0,93	93,46
	500	235	302	218	-428	104,5	84,73	0,94	94,72

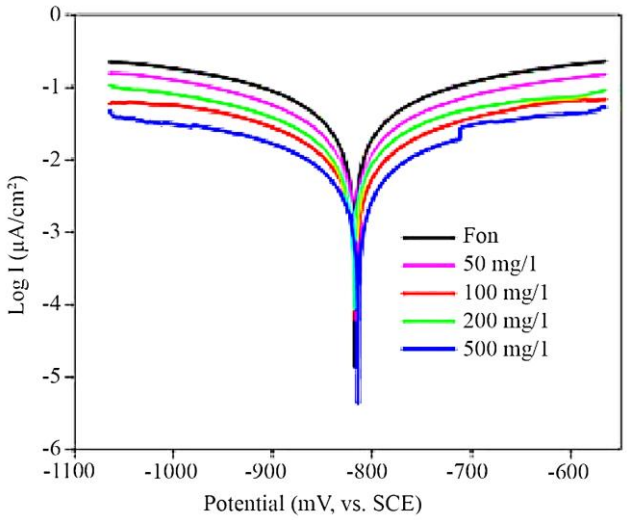

Fig. 6 Tafel plot of CT20 at different inhibitor concentrations in 1.0 M HCl solution at 298 K.

The equation can be used to calculate surface coverage and absorption efficiency %IE(EFM):

$$\%IE(EFM) = \theta \times 100 = \left(1 - \frac{i_{corr(inhibitors)}}{i_{corr(blank)}}\right) \times 100 \quad (3)$$

Where $i_{corr\ (inhibitors)}$ and $i_{corr\ (blank)}$ are corrosion current density.

According to Table 3 results, the I_{corr} values have decreased with increasing inhibitor concentration, indicating that when IE(EFM)) increases then these inhibitors can able to prevent corrosion by absorbing ST20 on the surface and forming physical and chemical bonds. As a result, the corrosion coefficient decreased and created a protective barrier. As per the EFM theory, the values of the causal factors (CF-2 and CF-3) were very close to their theoretical values (according to equations 2 and 3), indicating that the Tafel slopes and the corrosion current density were correct [24,25]. The polarization curves of St20 in 1 M HCl solution at 298 K with different inhibitor concentrations were determined using Equation 4.

$$\%IE\ (PDP) = \theta \times 100 = \left(1 - \frac{i_{corr(inhibition)}}{i_{corr(free)}}\right) \times 100 \quad (4)$$

Graphs (Figure 6) of the logarithm of the current density were used to draw the polarization curve. The results of corrosion properties, including corrosion potential (E_{corr}), corrosion current density (I_{corr}), anode and cathode Tafel slopes (If we plotted potential, E on the vertical axis and log i horizontally, the gradients would be equal to b_a and b_c.) and inhibition efficiency percent, %IE (PDP) are included in the table-3. It has revealed that with the increase in the concentration of inhibitors in the anode and cathode reaction process, the inhibition efficiency has increased significantly. Unsaturated bonds formed this protective barrier to the heteroatom and inhibitors on the surface of carbon steel. Depending on the type of reaction that often occurs in an acidic solution, the inhibitor can be an anode, cathode, or mixture.

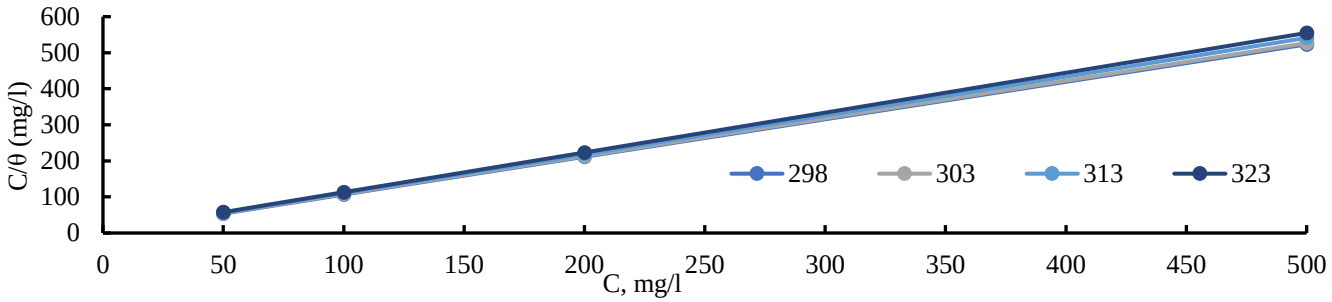

Fig. 7 Langmuir adsorption isotherms for St20 in 1.0 M HCl solutions at different concentrations of inhibitor at different temperatures.

The cathodic process in which hydrogen gas evolution is observed, the dissolution of metals, and the release of electrons also happen in the anodic process[26]. The plausible explanation is that the hydrogen evolution and electrochemical results usually confirm the potential ability of the metal dissolution process. In addition, by controlling the charge transfer charge, hydrogen gas developed in the cathodic reaction is successfully used as a variable to separate the contribution of hydrogen gas and hydroxyl ions to the cathodic delamination of the organic coating/inhibitor film[25, 27].

4.2. Thermodynamic and Kinetic Study of the Inhibition Process of Composite Corrosion Inhibitors

The graph has plotted of C/θ vs C against the four temperatures (298, 303, 313, and 323 K) in Figure 7, and curve intersections provided the calculation of C_{ads} values; these results are presented in Table 4. The obtained results showed that the adsorption of the selected compounds at the boundary of St20 steel/acid solution obeyed the Langmuir adsorption isotherm according to equations (5 and 6).

$$\frac{C}{\theta} = \frac{1}{K_{ads}} + C \quad (5)$$

$$K_{ads} = \frac{1}{55.5} = \exp\left(\frac{\Delta G^0_{ads}}{RT}\right) \quad (6)$$

It is clear from Table 4 data that the addition of inhibitors leads to negative values of ΔG^o_{ads}, which indicates the self-adsorption process of the studied MMF-1 corrosion inhibitors. When the value of ΔG^o_{ads} was up to -20 kJ/mol, then inhibition mostly depended on the electrostatic interaction between charged molecules and charged metal; that's why physical adsorption was mainly observed. However, we know the chemical sorption in which the formation of covalent bonds between the inhibitor molecules and the metal surface occurs at values of approximately -40 kJ/mol or less.

Table 5. Adsorption isotherm parameters of carbon steel electrode surface in 1.0 M HCl containing different inhibitor concentrations at different temperatures.

Inhibitor name	Temp. K	K_{ads} M^{-1}	ΔG^o_{ads} kJ·mol^{-1}
MMF-1	298	0,206	-29,462
	303	0,118	-30,735
	313	0,068	-30,121
	323	0,072	-29,482

According to Table 5, in our experiments, the ΔG^o_{ads} values exhibit a range from -29.456 to -30.735 kJ/mol, indicating that the adsorption of these MMF-1 compounds was two different types of interactions where chemical sorption and physical sorption were produced at the same time.

Since the temperature factors can change the actions of inhibitors and substrates in certain aggressive environments, Organic compounds dissolve more easily with increasing temperature. Thus, an increase in temperature can lead to a weakening of the corrosion resistance of metals. We studied the influence of this parameter on the performance of MMF-1, and we performed mass loss measurements at temperatures of 298, 303, 313, and 323 K. The results were summarized in Table-5, and the results were obtained after the samples were stored in water for 1 day.

In Table 5, it can be seen that the Corrosion Rate (C.R) in 1 M HCl solution was increased with increasing temperature. Conclusively, all inhibitor concentrations and the Corrosion Rate (C.R) increased with increasing temperature; however, lower values were observed at higher inhibitor concentrations. It means that IE% was increased as the temperature decreased. However, this evolution was more noticeable for the highest inhibitor concentrations [16].

Table 6. Values of activation parameters for carbon steel in 1.0 M HCl in the absence and presence of different concentrations of the studied inhibitor at different temperatures

Inhibitor	C, mg/l	Rs, (Ω cm^2)	Rct (Ω cm^2)	Y0 (Ω^{-1} s^{n}cm^{-2})	n	Cdl (μF cm^2)	θ	IE, EIS %
Without an inhibitor	0.0	0,4721	23,54	733,27	0,965	478,31	–	–
MMF-1	50	1,867	239,7	501	0,735	269,44	0,91	91,47
	100	1,094	284,7	278	0,765	186,86	0,93	93.27
	200	1,374	351,6	184	0,773	71,7	0,95	95,29
	500	1,142	396,1	101	0,802	21,64	0,96	96,18

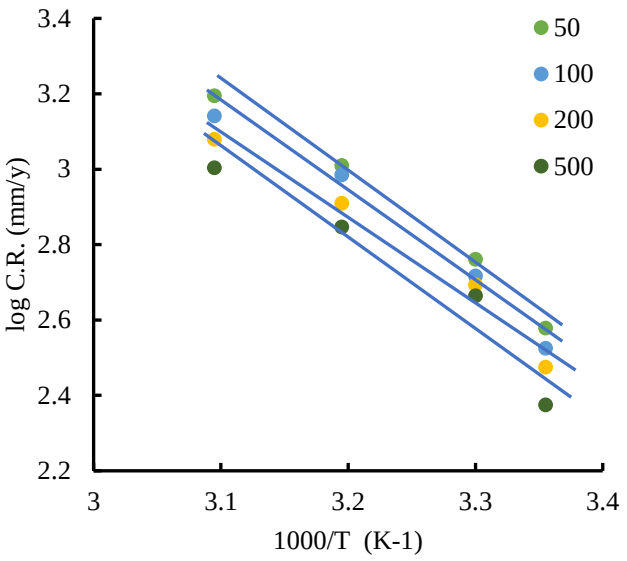

Fig. 8 Arrhenius plot for St20 steel in 1.0 M HCl solution of different concentrations of inhibitors

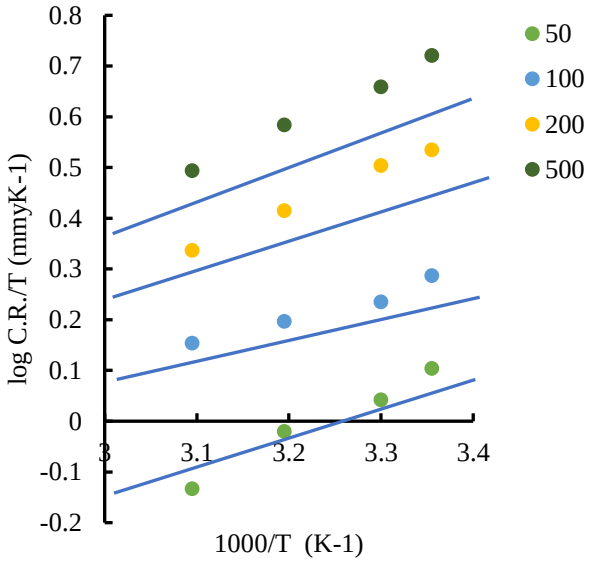

Fig. 9 Graphs of transition states for dissolution of St20 steel without inhibitors and in the presence of inhibitors

Using the Arrhenius equation, the activation energy of the corrosion process (E_a) was found based on equation (7) as follows.

$$logC.R. = \frac{-E_a}{2.303RT} + logA \quad (7)$$

R is the gas constant (8.31 J/mol/K), A is the pre-exponential Arrhenius factor, and T is temperature. At different concentrations of MMF-1, the probable activation energy (–Ea/2.303R) and the pre-exponential factor (A) were determined by linear regression between log(C.R) and 1/T. Table 6 and Figure 8 clearly show activation energy values without inhibitors and with certain concentrations of inhibitors at different temperatures. In the presence of an inhibitor, the E_a values have remained higher than the sample without the inhibitor. This behavior was fully characteristic of the case of physical adsorption of the inhibitor on the metal surface. However, the recovery rate was very low at higher temperatures, indicating that at these temperatures, the rate of inhibition of the physical sorption was faster than the rate of its formation. This phenomenon could also be explained by the fact that the corrosion process of steel in the presence of an inhibitor depended not only on the reaction occurring on the pure metal surface but also on the diffusion of iron ions through the adsorbed layer of the inhibitor. It was thus confirmed that a higher concentration of inhibitors participated in stronger physical absorption due to forming a stronger surface film and was, therefore, more effective. The values of kinetic parameters such as enthalpy (ΔH) and entropy (ΔS) of the corrosion process (8) can be estimated from the effect of temperature on the steel surface[24].

$$C.R. = \frac{RT}{N_A h} exp\left(\frac{\Delta S}{R}\right) exp\left(-\frac{\Delta H}{RT}\right) \quad (8)$$

where, h - Planck's constant, N_A - Avogadro's number.

The enthalpy and entropy values of the inhibitor compound MMF-1 on the surface of carbon steel were calculated using the transition state equation. Figure 9. shows the logarithm of (C.R./T) versus 1000/T, with a slope of -ΔH/2.303R and an intercept of [log(R/NAh) + (ΔS/2.303R)] gives straight lines. For carbon steel, the compounds were studied in the absence and presence of the inhibitor at concentrations of 50, 100, 200 and 500 mg/l in 1M HCl solution.

Table 3 shows that ΔH* values are positive. Positive values indicated the endothermic nature of the low-carbon steel melting process. The endothermic process also showed that the melting of steel has decreased at low temperatures and increased with increasing temperature. Negative ΔS* values indicated the formation of the activated complex in the rate-determining step, which revealed the association rather than the dissociation step, i.e., a decrease in the disorder has occurred during the transition from the reactants to the activated complex[8].

4.3. Scanning Electron Microscope (SEM) and Atomic Force Microscope (AFM) Analysis

The pre-corrosion, post-corrosion and inhibited states of the steel surface were studied using an SEM-EVO MA 10 (Zeiss, Germany) scanning electron microscope.The surface of samples of carbon steel at different concentrations was studied by the morphological SEM method. Figure 9 a shows the first photo of a steel sample cleaned with different sandpaper brands and washed in acetone. Microphotographs of the original steel sample were also taken using a scanning electron microscope in an environment without an inhibitor (Figure 9b) and with an inhibitor (Figure 9c).

Fig. 9a. Original photograph of the steel sample

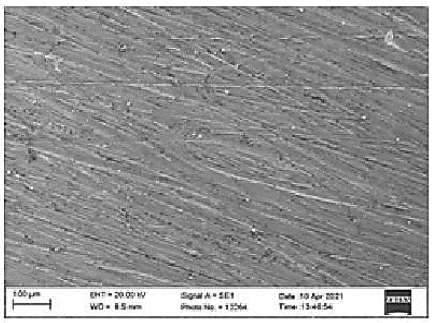

Fig. 9b. SEM photograph of a steel sample

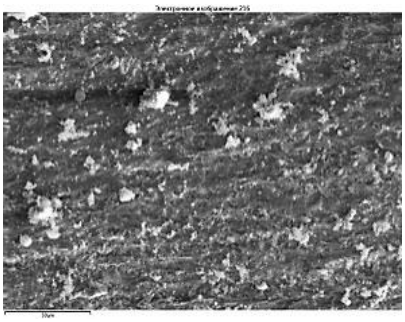

Fig. 9c. SEM photograph of inhibited steel sample

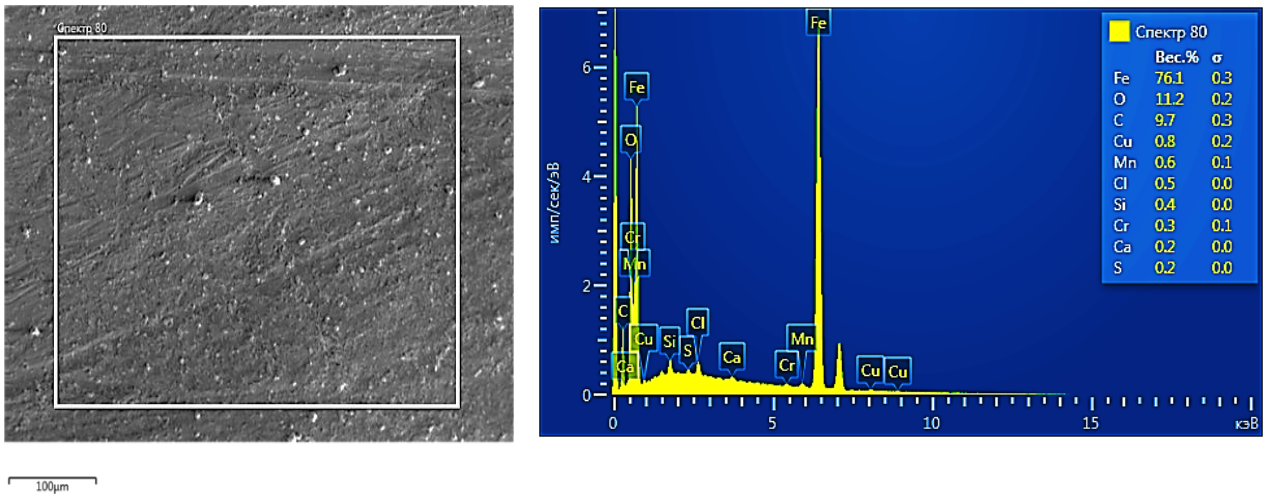

Fig.10 SEM and elemental analysis of the St20 sample inhibited with MMF-1 inhibitor

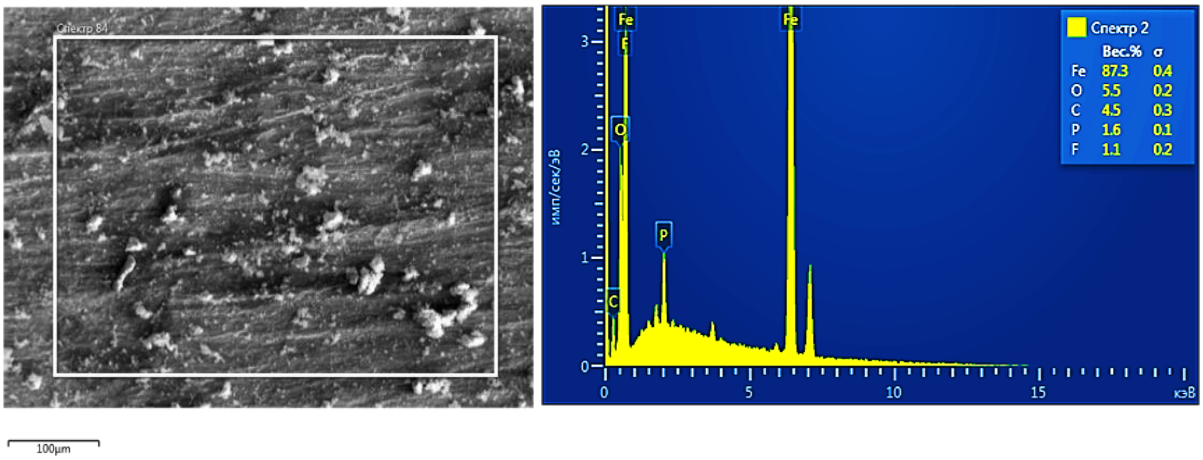

Fig. 11 SEM and elemental analysis of the St30 sample inhibited with MMF-1 inhibitor

Figure 10 presents the SEM and elemental analysis of MMF-1 brand corrosion. It was exhibited that the inhibitor was adsorbed on the steel surface and protected against aggressive environments. It has already been recognized from the element analysis. From Figure 11, we can see that the percentage of iron in the steel sample in the annealed solution was 87.3%. This indicates that the inhibitor showed a high level of protection of steel.The scan scale of the IEM is at the nano-micro scale, and it is a high-precision state-of-the-art device for studying the effects of inhibitors and their effects on the formation and prevention of corrosion at the metal/alloy interface.

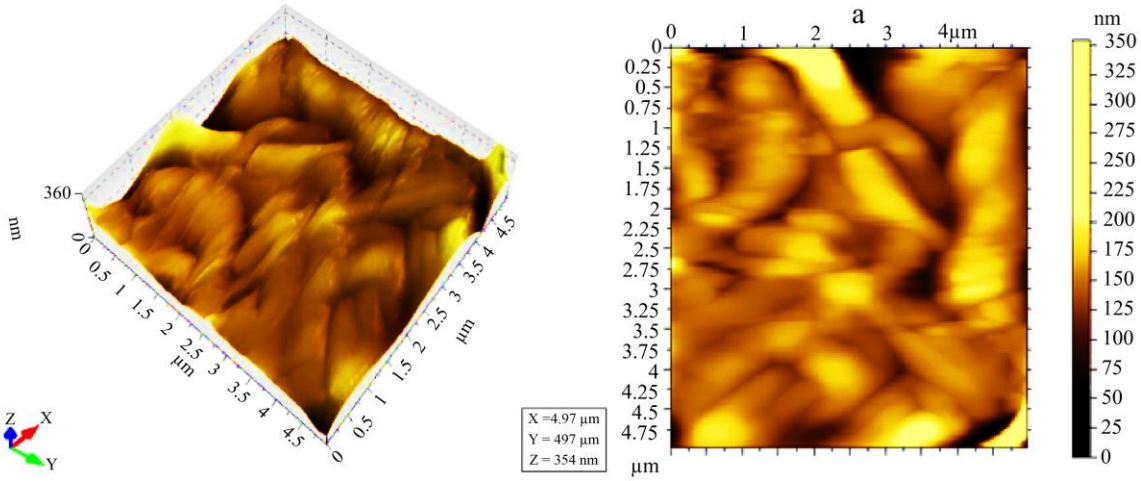

Fig. 12 A photomicrograph of the surface morphology of the St20 steel sample in Fon solution was obtained using an atomic force microscope

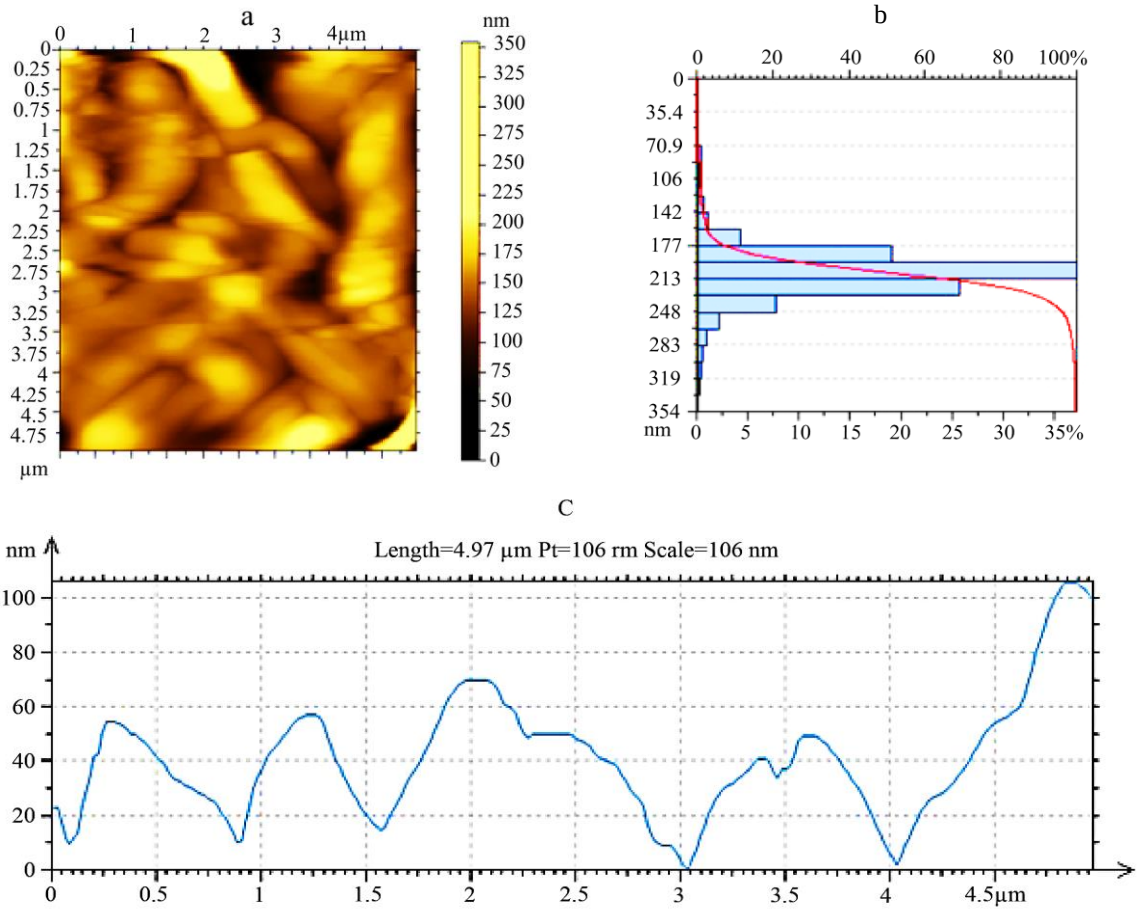

Fig. 13 Analysis of the topography of the steel surface

In Figure 12 we can see that the surface of the steel sample in the initial state of the carbon steel sample is almost flat, and there is no corrosion damage. This carbon steel surface was examined with a size of 4.5x4.5 mm; the size of the convex peaks was about 350 nm, and the size of the depressions was 135 nm (Figure 13a). From the analysis results, we found the surface scanning from 20 nm, 0 mm to 100 nm and 5mm. The waves appeared strongly to our eyes with a height of 106 nm on the surface of Pt106 nm (Figure 13c). It has followed the different concave and convex dimensions on the steel surface, and we have also determined the areas covered from the minimum coverage of 35% to 100% (Figure 13b).

5. Conclusion

The MMF-1 corrosion inhibitor based on methyl methacrylate, monoethanolamine, and phosphoric acid was obtained with a yield of 87%, and spectroscopic techniques firmly established its structure. Thermal and electrochemical properties have been studied as well. The main target of this work is to establish a new corrosion inhibitor in terms of efficiency against the corrosion process. The final postulations are made by authors who are listed below:

1. According to TG analysis it has revealed that the Significant mass loss interval was found at 22.58 – 140.3 °C, 140.3 – 509.3 °C and 509.3 – 800 °C, respectively. In addition, the highest heat output was shown at a temperature of 224.49 °C of Differential thermogravimetric analysis of MMF-1 composite corrosion inhibitor.
2. The noteworthy observation was that the obtained composite corrosion inhibitor has been established as 94.72% Inhibitor Efficiency (IE) based on the electrochemical analysis method.
3. Moreover, the inhibition mechanism of the composite corrosion inhibitor was studied, and it was evident that its inhibition efficiency increased with the increase in concentration. Its effect on the metal surface was also examined thoroughly by SEM and AFM on the inhibited steel surface.
4. Finally, MMF-1 corrosion inhibitor can easily be used commercially as a corrosion inhibitor based on its efficiency. However, the authors have suggested that further testing of the inhibitor's efficiency should be done before establishing it as a corrosion inhibitor.

Acknowledgements

The authors gratefully acknowledge the Termez State University and Termez Institute of Engineering and Technology.

Authors' Declaration

Conflicts of Interest: None.

I/We hereby confirm that all the Figures and Tables in the manuscript are mine/ours.

Authors' Contribution Statement

Choriev I.K: Writing – Original Draft. Turaev Kh. Kh: Reviewing and editing the paper. Normurodov B.A: Reviewing and editing the paper. Muzaffarova N. Sh: Software, Validation. Muzaffarova N. Sh: Writing – Original Draft, Conceptualization, Investigation, Visualisation.

References

[1] Chandrabhan Verma et al., "An Overview on Plant Extracts as Environmental Sustainable and Green Corrosion Inhibitors for Metals and Alloys in Aggressive Corrosive Media," *Journal of Molecular Liquids*, vol. 266, pp. 577-590, 2018. [CrossRef] [Google Scholar] [Publisher Link]

[2] Saviour A. Umoren et al., "A Critical Review on the Recent Studies on Plant Biomaterials as Corrosion Inhibitors for Industrial Metals," *Journal of Industrial and Engineering Chemistry*, vol. 76, pp. 91-115, 2019. [CrossRef] [Google Scholar] [Publisher Link]

[3] Marko Chigondo, and Fidelis Chigondo, "Recent Natural Corrosion Inhibitors for Carbon Steel: An Overview," *Journal of Chemistry*, vol. 2016, pp. 1-8, 2016. [CrossRef] [Google Scholar] [Publisher Link]

[4] P. Muthukrishnan, B. Jeyaprabha, and P. Prakash, "Mild Steel Corrosion Inhibition by Aqueous Extract of Hyptis Suaveolens Leaves," *International Journal of Industrial Chemistry*, vol. 5, pp. 1-11, 2014. [CrossRef] [Google Scholar] [Publisher Link]

[5] Jasdeep Kaur, Neha Daksh, and Akhil Saxena, "Corrosion Inhibition Applications of Natural and Eco-Friendly Corrosion Inhibitors on Steel in the Acidic Environment: An Overview," *Arabian Journal for Science and Engineering*, vol. 47, pp. 57-74, 2021. [CrossRef] [Google Scholar] [Publisher Link]

[6] Amel Kouache et al., "Experimental and Theoretical Studies of *Inula Viscosa* Extract as a Novel Eco-Friendly Corrosion Inhibitor for Carbon Steel in 1 M HCl," *Journal of Adhesion Science and Technology*, vol. 36, no. 9, pp. 988-1016, 2022. [CrossRef] [Google Scholar] [Publisher Link]

[7] Gang Lu et al., "Corrosion Protection of Iron Surface Modified by Poly(Methyl Methacrylate) Using Surface-Initiated Atom Transfer Radical Polymerization (SI-ATRP), *Colloid and Polymer Science*, vol. 288, pp. 1445-1455, 2010. [CrossRef] [Google Scholar] [Publisher Link]

[8] M.A. Shaymardanova et al., Study of Process of Obtaining Monopotassium Phosphate Based on Monosodium Phosphate and Potassium Chloride," *Chemistry Problems*, no. 3, pp. 279-293, 2023. [CrossRef] [Google Scholar] [Publisher Link]

[9] Fariborz Atabaki, Shahrzad Jahangiri, and Zohreh Pahnavar, "Thermodynamic and Electrochemical Investigations of Poly (Methyl Methacrylate–Maleic Anhydride) as Corrosion Inhibitors for Carbon Steel in 0.5 M HCl," *Protection of Metals and Physical Chemistry of Surfaces*, vol. 55, pp. 1161-1172, 2019. [CrossRef] [Google Scholar] [Publisher Link]

[10] Kh. S. Beknazarov et al., "The Inhibition of the Corrosion of Carbon Steel by Oligomeric Corrosion Inhibitors in Different Media," *International Polymer Science and Technology*, vol. 42, no. 4, pp. 33-38, 2015. [CrossRef] [Google Scholar] [Publisher Link]

[11] S. Kumar, "Eco-Friendly Corrosion Inhibitors: Synergistic Effect of Ethanol Extracts of Calotropis for Corrosion of Carbon Steel in Acid Media Using Mass Loss and Thermometric Technique at Different Temperature," *Protection of Metals and Physical Chemistry of Surfaces*, vol. 52, pp. 376-380, 2016. [CrossRef] [Google Scholar] [Publisher Link]

[12] Estela K.K. Baldin et al., "Ammonium Molybdate Added in Hybrid Films Applied on Tinplate: Effect of the Concentration in the Corrosion Inhibition Action," *Thin Solid Films*, vol. 600, pp. 146-156, 2016. [CrossRef] [Google Scholar] [Publisher Link]

[13] M. Mouanga et al., "A Localized Approach to Study the Effect of Cerium Salts as Cathodic Inhibitor on Iron/Aluminum Galvanic Coupling," *Corrosion Science*, vol. 90, pp. 491-502, 2015. [CrossRef] [Google Scholar] [Publisher Link]

[14] N. Rezaee, M.M. Attar, and B. Ramezanzadeh, "Studying Corrosion Performance, Microstructure and Adhesion Properties of a Room Temperature Zinc Phosphate Conversion Coating Containing Mn^{2+} on Mild Steel," *Surface and Coatings Technology*, vol. 236, pp. 361-367, 2013. [CrossRef] [Google Scholar] [Publisher Link]

[15] T.H. Muster et al., "A Combinatorial Matrix of Rare Earth Chloride Mixtures as Corrosion Inhibitors of AA2024-T3: Optimisation Using Potentiodynamic Polarisation and EIS," *Electrochemistry Acta*, vol. 67, pp. 95-103, 2012. [CrossRef] [Google Scholar] [Publisher Link]

[16] Nomozov Abror Karim Ugli et al., "Salsola Oppositifolia Acid Extract as a Green Corrosion Inhibitor for Carbon Steel," *Indian Journal of Chemical Technology*, vol. 30, no. 6, pp. 872-877, 2023. [CrossRef] [Google Scholar] [Publisher Link]

[17] I.A. Wonnie Ma et al., "A Concise Review on Corrosion Inhibitors: Types, Mechanisms and Electrochemical Evaluation Studies," *Journal of Coatings Technology and Research*, vol. 19, pp. 241-268, 2022. [CrossRef] [Google Scholar] [Publisher Link]

[18] M. Tourabi et al., "3, 5-Diaryl-4-Amino-1, 2, 4-Triazole Derivatives as Effective Corrosion Inhibitors for Mild Steel in Hydrochloric Acid Solution: Correlation between Anti-Corrosion Activity and Chemical Structure," *Protection of Metals and Physical Chemistry of Surfaces*, vol. 53, pp. 548-559, 2017. [CrossRef] [Google Scholar] [Publisher Link]

[19] Ahmed Al-Amiery, Wan Nor Roslam Wan Isahak, and Waleed Khalid Al-Azzawi, "Multi-Method Evaluation of a 2-(1,3,4-Thiadiazole-2-yl)Pyrrolidine Corrosion Inhibitor for Carbon sSteel in HCl: Combining Gravimetric, Electrochemical, and DFT Approaches," *Scientific Reports*, pp. 1-20, 2023. [CrossRef] [Google Scholar] [Publisher Link]

[20] I. Danaee, and P. Nikparsa, "Electrochemical Frequency Modulation, Electrochemical Noise, and Atomic Force Microscopy Studies on Corrosion Inhibition Behavior of Benzothiazolone for Steel API X100 in 10% HCl Solution," *Journal of Materials Engineering and Performance*, vol. 28, pp. 5088-5103, 2019. [CrossRef] [Google Scholar] [Publisher Link]

[21] Ahmed I. Adawy, Mohamed A. Abbas, and Khaled Zakaria, "New Schiff Base Cationic Surfactants as Corrosion Inhibitors for Carbon Steel in Acidic Medium: Weight Loss, Electrochemical and SEM Characterization Techniques," *Research on Chemical Intermediates*, vol. 42, pp. 3385-3411, 2016. [CrossRef] [Google Scholar] [Publisher Link]

[22] K.F. Khaled, and Mohammed A. Amin, "Computational and Electrochemical Investigation for Corrosion Inhibition of Nickel in Molar Nitric Acid by Piperidines," *Journal of Applied Electrochemistry*, vol. 38, pp. 1609-1621, 2008. [CrossRef] [Google Scholar] [Publisher Link]

[23] Chenrong Gu, Junying Hu, and Xiankang Zhong, "Evidence of Hydrogen Gas Evolution Accelerating the Cathodic Coating Delamination," *Corrosion Communications*, vol. 7, pp. 63-69, 2022. [CrossRef] [Google Scholar] [Publisher Link]

[24] Ambrish Singh et al., "Inhibition of Hydrogen Evolution and Corrosion Protection of Negative Electrode of Lead-Acid Battery by Natural Polysaccharide Composite: Experimental and Surface Analysis," *Journal of Energy Storage*, vol. 57, 2023. [CrossRef] [Google Scholar] [Publisher Link]

[25] Mohamed A. Abbas et al., "Synthesis, Characterization, Thermodynamic Analysis and Quantum Chemical Approach of Branched N, N′-Bis(p-Hydroxybenzoyl)-Based Propanediamine and Triethylenetetramine for Carbon Steel Corrosion Inhibition in Hydrochloric Acid Medium," *Arabian Journal for Science and Engineering*, vol. 48, pp. 7463-7484, 2023. [CrossRef] [Google Scholar] [Publisher Link]

[26] Abdelkarim Chaouiki et al., "Electrochemical Behavior and Interfacial Bonding Mechanism of New Synthesized Carbocyclic Inhibitor for Exceptional Corrosion Resistance of Steel Alloy: DFTB, MD and Experimental Approaches," *Arabian Journal of Chemistry*, vol. 15, no. 12, pp. 1-20, 2022. [CrossRef] [Google Scholar] [Publisher Link]

[27] Anees A. Khadom et al., "Kinetics and Synergistic Effect of Iodide Ion and Naphthylamine for the Inhibition of Corrosion Reaction of Carbon Steel in Hydrochloric Acid," *Reaction Kinetics, Mechanisms and Catalysis*, vol. 115, pp. 463-481, 2015. [CrossRef] [Google Scholar] [Publisher Link]